Article

Journal of the Brazilian Chemical Society

https://dx.doi.org/10.21577/0103-5053.20230177

J. Braz. Chem. Soc. **2024**, *35*, 5, e-20230177 , 1-14

Aminoguanidine Hydrazone Derivatives: The Antioxidant, Antineoplastic Profile, and Interaction with ctDNA Studies

Ari S. Guimarães,[a] Woodland S. Oliveira,[a] Aline R. S. Araújo,[b] Mary Ann Foglio,[b] Pedro G. V. Aquino,[c] João X. de Araújo-Júnior,[,d] Martine Schmitt,[e] Ana Lúcia T. G. Ruiz,[f] Isis M. Figueiredo[a] and Josué C. C. Santos[*,a]*

[a]*Instituto de Química e Biotecnologia, Universidade Federal de Alagoas, 57072-970 Maceió-AL, Brazil*

[b]*Faculdade de Ciências Farmacêuticas, Universidade Estadual de Campinas, 13083-970 Campinas-SP, Brazil*

[c]*Universidade Federal do Agreste de Pernambuco, 55292-278 Garanhuns-PE, Brazil*

[d]*Instituto de Ciências Farmacêuticas, Universidade Federal de Alagoas, 57072-900 Maceió-AL, Brazil*

[e]*Laboratoire d'Innovation Thérapeutique, UMR 7200, Université de Strasbourg, 60024-67401, Illkirch, France*

[f]*Centro Pluridisciplinar de Pesquisas Químicas, Biológicas e Agrícolas (CPQBA), Universidade Estadual de Campinas, 13148-218 Paulínia-SP, Brazil*

Herein, we report the synthesis and evaluation of four aminoguanidine hydrazone derivatives with different aromatic moieties. This class of compounds presents a series of biological applications. Derivative **AGH-3** with an indole nucleus offered the highest antioxidant capacity with results comparable to Trolox in 2,2-diphenyl-2-picrylhydrazyl radical ($DPPH^{\bullet}$), 2,2-azinobis(3-ethylbenzothiazoline-6-sulfonic acid ($ABTS^{\bullet+}$), Fe^{III} reduction assay (FRAP), and nitric oxide ($^{\bullet}NO$) radical scavenging assays. Furthermore, **AGH-3** showed the highest antiproliferative activity against human kidney cancer cells (786-0) with concentration necessary to inhibit 50% cell growth (GI_{50}) = 6.3 μM; additionally, in biophysical studies, **AGH-3** interacted with ctDNA (biological target model) forming a fluorescent supramolecular complex with a binding constant (K_b) of 2.89×10^3 M^{-1} with preferentially an intercalator mechanism. The tested compounds revealed the potential of aminoguanidine hydrazones as a strategic class of compounds with multitarget biological activity.

Keywords: aminoguanidine hydrazone, radical scavenging, *in vitro* cytotoxicity, DNA interaction

Introduction

Aminoguanidine hydrazones (AGHs) present a wide spectrum of applications, as a result of their mixed characteristics, in terms of electronic properties and ability to form hydrogen bonds with different systems.[1] Among the many biological activities reported for this class of compounds mentioned are: anticancer,[2] antioxidant,[3] antimicrobial,[4] inducible nitric oxide synthase (iNOS) inhibition,[5] antimalarial, and antitubercular activity.[6-8] Guanabenz (**1**) (Figure 1a) is an AGH α2-adrenergic receptor agonist that has been used as an antihypertensive agent since the 1970s,[9] attracting much attention. Among other properties reported are photoreceptor neuroprotective agent,[10] an adjuvant in the treatment of chronic toxoplasmosis,[11,12] as an acid-sensing ion channel modulator (ASICs) helping to control the pain of inflammatory diseases such as rheumatoid arthritis,[13] mitigating hepatotoxicity induced by acetaminophen,[14] and promotes glioblastoma cell sensitization under the action of the sunitinib antineoplastic agent.[15] Therefore, this compound may serve as a basis for developing active substances for an array of biological models. A good example is a monochlorinated derivative of guanabenz, called sephin-1 (**2**) (Figure 1a), which has attracted interest as a neuroprotective agent, especially since the compound presents no adrenergic effects.[16] Moreover, compound **2** has demonstrated other activities associated

*e-mail: josue@iqb.ufal.br; joao.araujo@icf.ufal.br
Editor handled this article: Hector Henrique F. Koolen (Associate)

with antivirals,[17] promoting modulation of acid-sensing ion channels and blocking acid-induced pain, a useful mechanism for pain control in inflammatory diseases.[13]

AGHs can block estrogen receptors, as compound **3** (Figure 1a), an estrogen receptor blocker capable of reversing breast cancer resistance to tamoxiphen.[18] Furthermore, compound **4** was tested against *Trypanosoma cruzi* (*T. cruzi*), with an LC_{50} (concentration necessary to kill 50% of the parasites) of 573 µM, considered moderate to low activity. Qualitative analysis of structure-activity relationships showed that the highest activity occurred with compounds carrying aromatic regions with *ortho* substitution and less exchangeable hydrogens.[19] The potential of compound **4** was featured by the ability to inhibit both the lipase from *Candida rugosa* and, for pest control, the crude intestinal lipase of *Rhynchophorus palmarum* larvae, a pest in agriculture.[20]

França *et al.*[21] demonstrated that AGH's **5**, **6**, **7** and **8** (Figure 1a) are active against strains of colon carcinoma (HCT-8), melanoma (MDA-MB-435), and glioblastoma (SF-295) with concentration necessary to inhibit 50% cell growth (GI_{50}) < 100 µM. Compound **5** was considered the least toxic compound when assessed against J774 macrophages. Compound **9** has demonstrated anti-inflammatory and analgesic activity via reduced release of proinflammatory cytokines, increased interleukin 10 (IL10) production, and reduced neuronal activity in mice.[22] Compound **9** can also reduce oxidative stress and presented anti-inflammatory action in a neonatal sepsis rodent model.[23] Finally, aminoguanidine derivatives were evaluated in different aromatic scaffolds against *T. cruzi* to demonstrate an LC_{50} from 17 to 876 µM. Compound **10** (Figure 1a) was the most active.

Based on the potentialities of aminoguanidine hydrazone and the interest in exploring the activities of the hydrazinoimidazoline group due to the wide range of biological activities, which include antimicrobial, antiproliferative,[24] antinociceptive,[25] anti-*T. cruzi*,[26] among others, AGHs contained that nucleus were designed and assessed. Besides, some compounds with five five-membered rings are described by their activity against some diseases, such as compound **11**, which presented LC_{50} from 0.1 to 1 µM,[27,28] about 500 more active than compound **4**. Thus, in this work, compounds incorporating aromatic or heterocyclic groups to the hydrazinoimidazoline nucleus were synthesized (Figure 1b), and antiproliferative and antioxidant activities were reported, as well as biophysical studies in modified analogs exploring deoxyribonucleic acid (DNA) model were carried out to establish a potential target.

Experimental

Reagents and solutions

All reagents and solvents used in this work presented an analytical degree of purity (≥ 95%), being used directly without further purification. In the antioxidant assays, compounds 2,2-azinobis(3-ethylbenzothiazoline-6-sulfonic acid (ABTS), 2,2-diphenyl-2-picrylhydrazyl radical (DPPH•), quercetin, and Trolox were purchased from Sigma-Aldrich (Saint Louis, MO, USA). In the antiproliferative tests, bovine serum albumin (BSA), streptomycin-penicillin, dimethyl sulfoxide (DMSO), 3-(4,5-dimethylthiazolyl-2)-2,5-diphenyltetrazolium bromide (MTT), fetal bovine serum, trichloroacetic acid (TCA), H_3PO_4 and sulforhodamine B were purchased from Sigma-Aldrich (Saint Louis, MO, USA). In the biophysical interaction studies, Tris-HCl, ethidium bromide (EB), Hoechst 33258 (HO), and ctDNA (Calfthimus) type I fibers were used from Sigma-Aldrich (Missouri, USA). At the

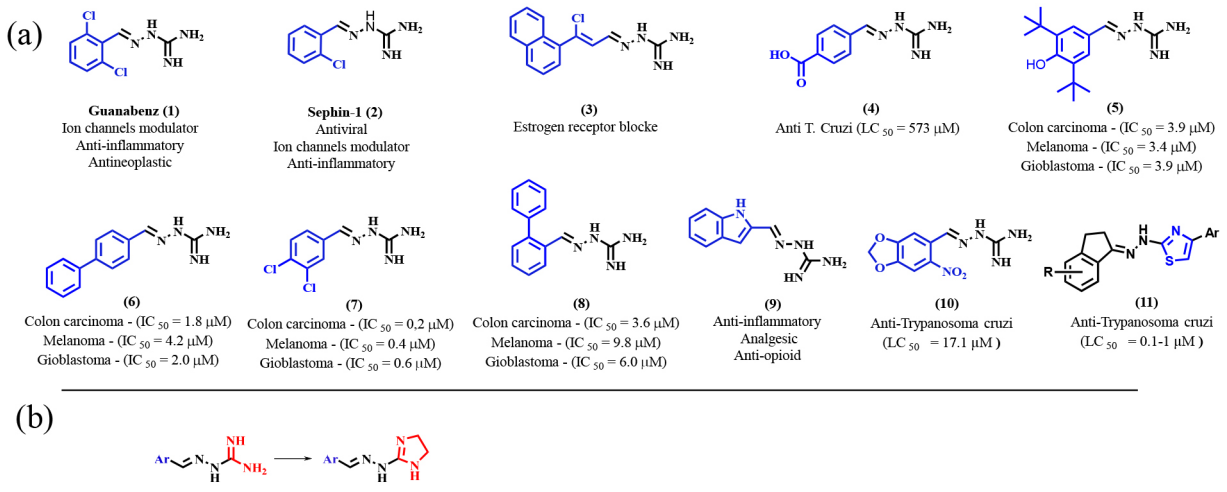

Figure 1. (a) Some examples of bioactive AGHs in the literature. (b) Proposed modification in the aminoguanidine nucleus system.

same time, potassium persulfate ($K_2S_2O_8$) was purchased from Merck (Darmstadt, Germany).

DPPH$^{\bullet}$ stock solution was prepared by dissolving 12 mg of the commercial radical in 50 mL of methanol. The ABTS$^{\bullet+}$ stock solution (1 mmol L^{-1}) radical was prepared by directly dissolving 26 mg of ABTS in water, then 3.0 mL of 1 mmol L^{-1} $K_2S_2O_8$ were added, completing the volume of 10 mL with deionized water. After 16 h of incubation protected from light, the solution was diluted to 25 mL with 0.05 mol L^{-1} phosphate buffer (pH = 7.2).[29,30]

The ctDNA stock solution was prepared by dissolving an appropriate amount of solid nucleic acid in Tris-HCl buffer solution overnight and storing it at 4 °C in the dark. The concentration of the stock ctDNA solution was determined using UV absorption at 260 nm and an extinction coefficient (ε) of 6600 L mol^{-1} at 25 °C. The purity of the ctDNA solution was evaluated by monitoring the absorbance ratio from 260 to 280 nm. If the solution gave a ratio of $A_{260}/A_{280} > 1.8$, the ctDNA was considered sufficiently free from protein contamination.[31]

Apparatus

Analytical thin layer chromatography (TLC) was performed using silica gel plates Merck (Darmstadt, Germany) 60F 254, and plates were visualized by exposure to ultraviolet light. Compounds were purified on reverse phase column: adsorption via hydrophobic interaction (AIT) 50 g (C18). Yields refer to isolated compounds estimated to be > 95% pure as determined by ^{1}H nuclear magnetic resonance (NMR) or high performance liquid chromatography (HPLC). The ^{1}H and ^{13}C NMR spectra were recorded on Bruker Advanced DPX Spectrometer (Bruker Corporation, Billerica, USA) operating at 400 and 100 MHz, respectively. For retention time (t_R) and purity degree (%) of all compounds, a Shimadzu HPLC chromatograph (model SIL-20AHT, Kyoto, Japan) was used with a Luna® (5 μm C_{18}(2) 100 Å) column (250 × 4.6 mm) and wavelength (λ) of 254 nm (photodiode array (PDA) detector). During all HPLC analyses, a mixture of methanol/trifluoroacetic acid with HPLC degrees (≥ 99%) was used as a mobile phase (v/v 99.9:0.1%). Moreover, some parameters were established as (*i*) sample concentration of 1 mg mL^{-1}, (*ii*) the flow rate of 1 mL min^{-1}, (*iii*) run time of 10 min, and (*iv*) injection volume of 5 μL. Lastly, t_R and absorbance values were computed in minutes (min) and milliabsorbance unities (mAU). All spectral and chemical characterization data are described in the Supplementary Information section.

The pH measurements were performed using a Gehaka pH meter (PG1800 model, Brazil). Molecular absorption measurements were performed in a scanning spectrophotometer Micronal (AJX-6100PC model, São Paulo, Brazil) with a double-beam and equipped with 1 cm optical path quartz cuvettes. The spectrofluorimetric titrations were performed on a Shimadzu spectrofluorimeter (model RF-5301PC, Kyoto, Japan) equipped with a Xe lamp (150 W) and using 1 cm optical path quartz cuvettes.

Synthesis and characterization

Synthesis of 2-hydrazinyl-4,5-dihydro-1*H*-imidazole iodide (**14**)

2-Hydrazine-4,5-dihydro-1*H*-imidazole iodide (**14**) was prepared by dissolving 4 mmol (976.4 mg of methylthioimidazole iodate (**12**, 244.1 g mol^{-1}) in 8 mL ethanol, followed by the addition of 4.4 mmol (344.2 mg) hydrazine hydrate (**13**, 50.6 g mol^{-1}) (Scheme 1). The mixture was stirred under reflux for 7 h and monitored using TLC. The reaction was then cooled and evaporated until dry, followed by the addition of ethyl ether and filtration of the white precipitate formed,[32] 2-hydrazine-4,5-dihydro-1*H*-imidazole iodide (**14**).[33,34] 228.03 g mol^{-1}; yield 778 mg (3.4 mmol, 85%); t_R 4.84 min; purity: 54.35%; ^{1}H NMR (400 MHz, DMSO-d_6) δ 3.56 (s, 4H, 2 × CH_2CH_2), 6.70-8.50 (brs, 4H, 4 × NH, NH_2); ^{13}C NMR (100 MHz, DMSO-d_6) δ 162.25 (C), 43.00 (CH_2CH_2), (Figures S1, S2, and S11, Supplementary Information section).

Synthesis of AGH derivates (**AGH-1** to **AGH-4**)

An appropriate aldehyde 0.4385 mmol (1.0 eq.) was added to a mixture of 0.4385 mmol (1.0 eq.) of compound **14** dissolved in ethanol. The resulting mixture was refluxed (6 h) until consumption of the aromatic aldehyde (**15**-**18**) (Scheme 1), indicated by the disappearance of its corresponding line in the TLC analysis.[35] The compounds were purified by reversed-phase flash column chromatography. Finally, the hydrochloride salts were obtained after salification with 2 M HCl in Et_2O. The resulting solids were washed twice with Et_2O and dried at room temperature under reduced pressure. The final compounds were characterized using NMR spectroscopy (^{1}H and ^{13}C NMR). The purity of each compound was over 95%, as determined by HPLC.

4-((2-(4,5-Dihydro-1*H*-imidazol-2-yl)hydrazinylidene) methyl)-benzoic acid hydro-chloride (**AGH-1**)[32]

Yellow solid; multi-plane light conversion (MPLC) inverse (MeOH 40%); 268.7 g mol^{-1}; yield 110 mg (0.41 mmol, 93%); t_R 2.38 min; purity: 100%; ^{1}H NMR (400 MHz, DMSO-d_6) δ 3.76 (s, 4H, CH_2CH_2), 7.87-8.08 (m, *J* 8.0 Hz, 4 aromatic H), 8.26 (s, 1H, ArCH=N), 8.79 (s, 1H, NH), 10.90

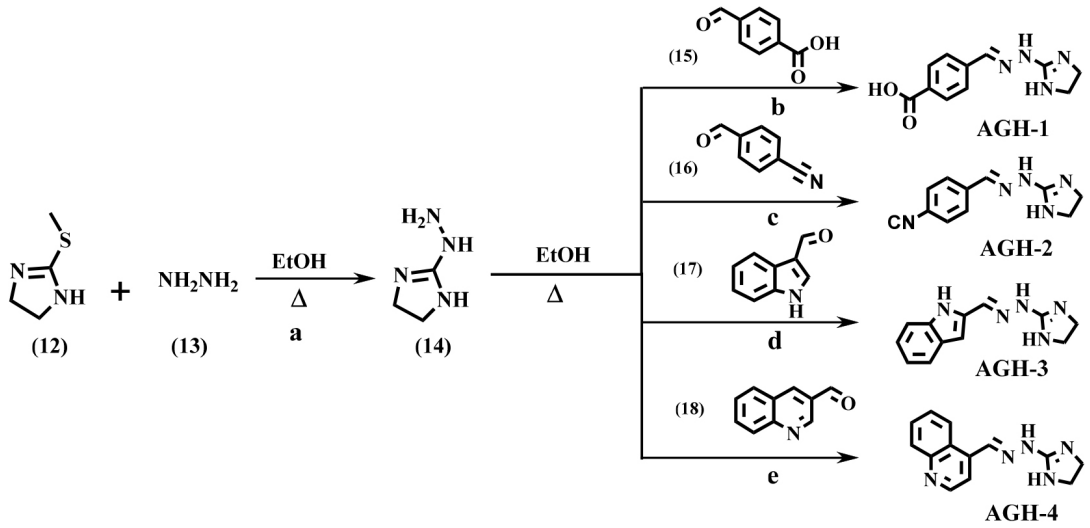

Scheme 1. Synthesis of AGH derivates **AGH-1** to **AGH-4**. (a) Methylthioimidazole iodate (**12**, 244.1 g mol^{-1}) and hydrazine hydrate (**13**, 50.6 g mol^{-1}) in 8 mL ethanol were stirred under reflux for 7 h forming 2-hydrazine-4,5-dihydro-1*H*-imidazole iodide (**14**, 228.03 g mol^{-1}) (yield 85%); (b) The mixture of 4-formylbenzoic acid (**15**, 150.13 g mol^{-1}) and **14** was refluxed (6 h) forming **AGH-1** (yield 93%); (c) mixture 4-formylbenzonitrile (**16**, 131.13 g mol^{-1}) and **14** was refluxed (6 h) forming **AGH-2** (yield 64%); (d) mixture 1*H*-indole-3-carbaldehyde (**17**, 145.16 g mol^{-1}) and **14** was refluxed (6 h) forming AGH-3 (yield 64%); (e) mixture quinoline-3-carbaldehyde (**18**, 157.17 g mol^{-1}) and **14** was refluxed (6 h) forming **AGH-4** (yield 65%).

(s, 1H, NH), 12.44 (s, 1H, COOH); ^{13}C NMR (100 MHz, DMSO-d_6) δ 43.30 (CH_2CH_2), 128.04, 130.07 (aromatic CH), 132.70, 137.72 (aromatic C), 147.50 (ArCH=N), 158.32 (C=N, imidazole), 167.29 (C=O) (Figures S3, S4 and S12, Supplementary Information section).

4-((2-(4,5-Dihydro-1*H*-imidazol-2-yl)hydrazineylidene) methyl)benzonitrile hydro-chloride (**AGH-2**)

White solid; column chromatography (MeOH:CH_2Cl_2 1:9); 249.7 g mol^{-1}; yield 70 mg (0.28 mmol, 64%); ^{1}H NMR (400 MHz, DMSO-d_6) δ 3.77 (s, 4H, CH_2CH_2), 7.96 (d, *J* 8.5 Hz, 2 aromatic H), 8.05 (d, *J* 8.5 Hz, 2 aromatic H), 8.23 (s, 1H, ArCH=N), 8.79 (brs, 1H, NH), 12.47 (s, 1H, NH); ^{13}C NMR (100 MHz, DMSO-d_6) δ 43.30 (CH_2CH_2), 112.95, 119.04 (aromatic CH), 128.57, 133.14 (aromatic C), 138.16 (cyano group), 146.69 (ArCH=N), 158.38 (C=N) (Figures S5 and S6, Supplementary Information section).

2-((2-(4,5-Dihydro-1*H*-imidazol-2-yl)hydrazineylidene) methyl)-1*H*-indole hydro-chloride (**AGH-3**)

Brown solid; column chromatography (MeOH:CH_2Cl_2 1:9); 263.73 g mol^{-1}; yield 0.50 g (2.65 mmol, 72%); ^{1}H NMR (400 MHz, DMSO-d_6) δ 3.74 (s, 4H, CH_2CH_2), 7.15 (t, 1H, *J* 7.9 Hz), 7.22 (t, 1H, *J* 7.5 Hz), 7.45 (d, 1H, *J* 8.0 Hz), 7.89 (d, 2H, *J* 2.8 Hz), 8.34 (d, *J* 7.8 Hz, 1H), 8.45 (s, 1H, ArCH=N), 11.86 (brs, 1H, NH), 12.46 (s, 1H, NH imidazole); ^{13}C NMR (100 MHz, DMSO-d_6) δ 43.26 (CH_2CH_2), 112.31, 121.12, 123.00, 123.26 and 132.48 (aromatic CH), 146.43 (ArCH=N), 110.98, 124.31 and 137.57 (aromatic C), 157.75 (imidazole C) (Figures S7 and S8, Supplementary Information section).

4-((2-(4,5-Dihydro-1*H*-imidazol-2-yl)hydrazineylidene) methyl)quinoline hydro- chloride (**AGH-4**)[36]

Yellow solid; column chromatography (dichloromethane (DCM):MeOH 5%); 275.74 g mol^{-1}; yield 79 mg (0.29 mmol, 65%); t_R 2.38 min; purity: 95.26%; ^{1}H NMR (400 MHz, DMSO-d_6) δ 3.81 (s, 4H, CH_2CH_2), 7.96 (t, 1H, *J* 7.7 Hz), 8.10 (t, 1H, *J* 7.7 Hz), 8.40 (d, 1H, *J* 8.5 Hz), 8.49-8.50 (m, 1H, *J* 5.3 Hz), 8.57 (s, 1H, ArCH=N), 9.27 (d, *J* 5.3 Hz, 1H), 9.31 (s, 1H, imidazole NH), 13.61 (s, 1H, hydrazine NH); ^{13}C NMR (100 MHz, DMSO-d_6) δ 43.42 (CH_2CH_2), 119.12, 124.75, 129.79, 133.22, 143.02 (aromatic CH), 146.64 (ArCH=N), 125.79 (aromatic C), 158.23 (imidazole C) (Figures S9, S10, and S13, Supplementary Information section).

Antioxidant activity assays

DPPH$^\bullet$ radical scavenging assay

In order to evaluate the DPPH$^\bullet$ radical scavenger capacity, 0.20 mL of DPPH$^\bullet$ radical (608 μmol L^{-1}) was mixed incrementally with the sample or reference solution (1-50 mg L^{-1}), and the final volume was adjusted to 4.0 mL using 30% (v/v) hydroethanolic solution. After 30 min of incubation without light, the spectrophotometric measurement was made at 527 nm. The concentration required to reduce 50% of the radical specie (IC_{50}) value was determined using a linear regression between the concentration in mg L^{-1} (abscissa axis) and the percentage inhibition (I) (ordinal axis), using the equation $I / \% = [1 - (A_{AO}/A_{ref}) \times 100]$, where A_{AO} corresponds to sample absorbance and A_{ref} the negative control absorbance (0.20 mL of DPPH$^\bullet$ solution and 3.8 mL hydroethanolic solution 30% (v/v)).[29,30]

ABTS$^{\bullet+}$ radical scavenging assay

To perform the ABTS$^{\bullet+}$ radical assay, we proceeded as follows: 0.22 mL of the ABTS$^{\bullet+}$ radical solution was added incrementally to the sample or standard solution (1-50 mg L^{-1}), and 2.80 mL of deionized water. After 15 min, the spectrophotometric measurement was done 734 nm. The reference signal was obtained from a similar solution; thus, the sample was replaced with water. The IC_{50} value was determined using a linear regression between the concentration in mg L^{-1} (abscissa axis) and the percentage inhibition (I) (ordinal axis), using the equation $I / \% = [1 - (A_{AO}/A_{ref}) \times 100]$; with A_{AO} as the sample absorbance and A_{ref} as the negative control absorbance (0.20 mL of ABTS$^{\bullet+}$ solution and 3.8 mL of deionized water).[29,30]

Fe^{III} reduction assay (FRAP)

Evaluation of Fe^{III} reduction capacity was performed by adding 0.75 mL of sample or standard solutions, 1.25 mL of $K_3[Fe(CN)_6]$ at 1.0% (m/v) previously diluted in phosphate buffer pH 6.0, and 1.25 mL of ultrapure water. The mixture was incubated for 20 min at 50 °C. Then, 1.25 mL of trichloroacetic acid 10% (v/v) and 0.5 mL of $FeCl_3$ 0.1% (m/v) were added to form the Prussian Blue complex (chromophore), which presents a maximum absorbance at 700 nm. The reference solution (analytical blank) was prepared by replacing the standard or sample with ultrapure water.[37]

Nitric oxide (•NO) scavenger

To evaluate •NO radical scavenging, 0.5 mL of 5.0 mmol L^{-1} sodium nitroprusside solution diluted in phosphate buffer (0.1 mol L^{-1}, pH 7.0) and 2.5 mL of the samples or standards were used. The final volume was adjusted to 5.0 mL with ultrapure water, and the resulting solution was incubated at room temperature for 150 min.[38] The reference signal (blank) was obtained from a solution similar to the one above; however, the sample or standard was replaced by ultrapure water. At 30 min intervals, 1.0 mL aliquots of the incubated samples were collected and mixed with 1.0 mL of Griess reagent. The chromophore was generated from the sulfanilamide-sodium nitrite diazonization reaction in an acidic medium, followed by coupling with naphthyl ethylenediamine and measured spectrophotometrically at 546 nm.

Antiproliferative activity

Cell lines

Nine human cancer cell lines were used: U251 (glioblastoma); MCF-7 (adenocarcinoma of the breast); NCI-ADR/RES (multidrug-resistant ovarian adenocarcinoma); 786-0 (adenocarcinoma of the kidney); NCI-H460 (non-small cell carcinoma of the lung); PC-3 (adenocarcinoma of the prostate); OVCAR-03 (adenocarcinoma of the ovary); HT-29 (colorectal adenocarcinoma); K562 (chronic myelogenous leukemia) and one immortalized cell line (HaCat, human keratinocyte). Stock cultures were grown in the complete medium Roswell Park Memorial Institute (RPMI)-1640 supplemented with 5% fetal bovine serum (FBS, Nutricell, Rio de Janeiro, Brazil) and penicillin:streptomycin (1000 mg mL^{-1}:1000 U mL^{-1}) at 37 °C and 5% of CO_2. All experiments were done with the cell at 5 to 12 passages.

Sample preparation

Aliquots of **AGH-1**-**AGH-4** were diluted in DMSO (100 mg mL^{-1}) followed by serial dilution in a complete medium affording the final concentrations of 0.25, 2.5, 25, and 250 μg mL^{-1}. Doxorubicin was diluted in the same way affording the final concentrations (0.025, 0.25, 2.5, and 25 μg mL^{-1}).

Treatment and evaluation

Each cell line was plated in 96-well plates (100 μL *per* well, cell density from 3 to 6×10^3 cell *per* well) for 24 h before samples addition (100 μL *per* well, **AGH-1**-**AGH-4**; 0.25 to 250 μg mL^{-1}) in triplicate and incubated for 48 h. Doxorubicin (0.025 to 25 μg mL^{-1}) was used as a positive control. Before (T_0) and after (T_1) sample addition, the cells were fixed with trichloroacetic acid (TCA, 50% (v/v), 50 μL *per* well), and cell proliferation quantification was determined by sulforhodamine B (SRB) protocol at 540 nm. The difference between T_1 and T_0 absorbance values represented 100% of cell proliferation, and each cell line's proliferation (%) in the presence of each sample concentration was calculated. The results were plotted as cell growth *versus* sample concentration. Thus, using these curves, the sample concentration required to promote 50% of growth inhibition (GI_{50}) of each cell line was calculated by sigmoidal regression using Origin 9.0 software.[39] The selectivity index (SI) was calculated as $SI = GI_{50(HaCaT)}/GI_{50\ tumor\ cell}$.[31,40,41]

DNA interaction studies

Evaluation of ctDNA-ligand interaction using UV-Vis and molecular fluorescence

Absorbance measurement was performed for **AGH-3** (10 μM), ctDNA (0-120 μM), and the respective mixture to evaluate the complex formation. The UV-Vis spectra were recorded in the 220-330 nm range. The spectrofluorometric

titrations were performed, keeping **AGH-3** concentration constant (10 μM) and varying the ctDNA in incremental additions. The excitation wavelength was 310 nm, respectively using 5 and 10 nm slits (for excitation and emission), with the spectra recorded from 320 to 500 nm.

Competition study with ethidium bromide (EB) and Hoechst (HO)

To evaluate the preferential binding mode with the ctDNA, the final concentration of the fluorescent probes and the ctDNA was fixed ([EB] = [HO] = 1.0 μM and [ctDNA] = 10 μM) and incrementally increasing **AGH-3** (1 to 340 μM). Each system was used in a specific excitation wavelength for the molecular fluorescence measurements: EB-ctDNA (λ_{ex} = 525 nm) and HO-ctDNA (λ_{ex} = 353 nm).

DNA melting point (T_m)

In the denaturation temperature (T_m) assay, the ctDNA was slowly heated in a range of 24 to 95 °C in the absence and presence of **AGH-3** (20 μM). The differing system absorbance values were monitored at 260 nm. The variation equation of T_m [$\Delta T_m = T_{m\ (ligand)} - T_{m\ (ctDNA)}$] was adopted to assess the binding mode. The T_m values were determined based on the mid-point on a graphic representation of f_{ss} *vs.* temperature, which is defined as $f_{ss} = [(A - A_0)/(A_f - A_0)]$, f_{ss} corresponds to the ctDNA single strand fraction, A_f and A_0 respectively represent the maximum (single-stranded DNA) and minimum (DNA double-strand) absorbance values at 260 nm.[42]

Molecular docking

The structures of the compounds were drawn and converted into three-dimensional MDL Molfile (.mol) files from ChemDraw 15.1 software (Massachusetts, USA).[43] Afterwards, the compounds were optimized using the Austin Model 1 (AM1) method from MOPAC software (Colorado, USA),[44] generating the input in the Mercury 4.3.1 graphical user interface.[45] The final structures were converted into pdbqt format in AUTODOCK TOOLS v. 1.5.6 (California, USA).[46] DNA macromolecule structure (PDB ID: 1BNA) was obtained from the Protein Data Bank (PDB). Subsequently, all ligands, ions and water molecules that were present in the original structure of the biomolecule referring to the PDB file were manually removed, polar hydrogen atoms added, partial atomic charges were calculated as well as the AD4 designation of the atoms and the final structures were converted into pdbqt format using the AUTODOCK TOOLS v. 1.5.6.[46] Auto Grid was used to set the coordinates and for DNA (PDB ID: 1BNA) blind docking was performed.[47] All docking calculations were performed using Autodock vina software[46] and the output results were rendered in Discovery Studio Visualizer (San Diego, California, USA) software[48] and UCSF Chimera (San Francisco, California, USA).[49]

Statistical analysis

Data were expressed as mean ± standard deviation (SD) considering triplicate measurements (n = 3). Analysis of variance (ANOVA) was employed as a hypothesis test, and when necessary, Tukey's test was used ($p = 0.05$). Statistical evaluations were performed using OriginPro 9.0 software (OriginLab Corporation, Northampton, Massachusetts, USA).[39]

Results and Discussion

Synthesis

The compounds evaluated in this study were synthesized in two steps (Scheme 1). First, the key hydrazinyl-imidazole intermediate **14** was synthesized by condensation of the commercially available 2-(methylmercapto)-2-imidazoline (**12**) with hydrazine hydrate **13**. The intermediate **14** was then condensed with the appropriate aldehyde (compounds **15-18**), resulting in **AGH-1** to **AGH-4** derivatives with yields ranging from 64 to 93%. The final compounds were characterized using NMR spectroscopy (^{1}H and ^{13}C NMR). The purity of each compound was over 95%, as determined by HPLC (Figures S11 to S13, Supplementary Information section). The spectroscopic data of compounds **14**, **AGH-1** and **AGH-4** were identical to those reported in the literature.[32-34,36] The ^{1}H NMR data demonstrated the formation of intermediate **14** by the disappearance of the signal corresponding to the methylene hydrogens of the methylmercapto function of compound **12** at approximately δ 3.0 ppm and the appearance of the signals corresponding to the hydrogens of the added amine groups, between δ 6.65-9.03 ppm. For the compounds **AGH-1**-**AGH-4**, the presence of a singlet between δ 8.23-8.31 ppm corresponding to the imine hydrogen was observed.

Antioxidant activity

Evaluation of antioxidant capacity for the aminoguanidine derivatives **AGH-1-AGH-4** was performed using DPPH$^{\bullet}$, ABTS$^{\bullet+}$, and $^{\bullet}$NO radical scavenging assays, and FRAP assay (Table 1 and Figure 2). In this evaluation, the positive controls gallic acid (phenolic acid), Trolox (vitamin E mimetic), quercetin (flavonoid) and caffeic acid (conjugated phenolic acid), antioxidant compounds of different classes and degrees of lipophilicity, were used.

For the DPPH$^{\bullet}$ radical assay, the **AGH-3** derivative was the most active of the compounds evaluated, with an IC_{50}

value lower than that of Trolox (Table 1). Nevertheless, the **AGH-2** was 2-3 times less effective than positive controls. Sztanke *et al.*[50] observed similar results for various hydrazinoimidazoline derivatives using the DPPH• radical assay. Baldisserotto *et al.*[51] obtained IC_{50} values between 10.9 to 7113 μmol TE (Trolox equivalent) g^{-1} for indole derivatives. Similarly, in the ABTS•+ assay, **AGH-3** presented the lowest IC_{50} of the series of compounds evaluated, with higher efficacy compared to Trolox, presenting an IC_{50} of 2-7 times more elevated than the phenolic acids and quercetin. Faillace *et al.*[52] found differing results for sulfur and oxygenated imidazolines, in which 500 μM of the compounds were needed for ABTS•+ radical inhibition percentages of 22 to 99%.

As for the iron reduction method (FRAP), **AGH-3** was the most efficient compound (0.496 ± 0.010) of the evaluated series, reaching an activity comparable to the Trolox standard (0.515 ± 0.030). Furthermore, after normalizing the values (A_{700}/μM), **AGH-3** exhibited activity similar to caffeic acid and gallic acid standards. Baldisserotto *et al.*[51] evaluating compounds with the indole nucleus, achieved values of 15.1 at 12049 μmol TE g^{-1} of iron reduction. Mihailovi *et al.*[53] achieved results similar to **AGH-1-AGH-4** for diacylhydrazine derivatives and 1,3,4-oxadiazoes in absorbance units (0.173 to 0.478).

Because of its crucial role in the inflammatory process, in addition to carcinogenic processes, the •NO radical is a pro-oxidant species that demands attention since inhibitors of this species represent a significant therapeutic advance, especially in controlling inflammatory diseases.[54] Thus, the •NO radical scavenging capacity of **AGH-3** (more active in previous assays) was evaluated using Trolox as a standard (Figure 2). The antioxidant capacity was analyzed for 150 min. Initially (time zero), **AGH-3** and Trolox inhibited approximately 38% of the generated radical; however, the inhibition of **AGH-3** was 22.3% lower than the standard.

The difference in radical scavenging activity among the four compounds evaluated could have a relationship to the presence of different substituents in the aminoguanidine moiety. Notably, the presence of an indole aromatic

Table 1. Antioxidant capacity of aminoguanidine derivatives and standards, measured by DPPH•, ABTS•+ and FRAP methods

Compound	Antioxidant capacity			
	IC_{50} / μM		FRAP (A_{700}, 10 mg mL^{-1})	FRAP[a] (normalized)
	DPPH•	ABTS•+		
AGH-1	1160 ± 37[a]	33.4 ± 11.9[a,b]	0.375 ± 0.050[a]	2.02 ± 0.27[a]
AGH-2	273 ± 3[b]	47.3 ± 4.[4]c	0.367 ± 0.010[a]	1.83 ± 0.05[a]
AGH-3	48.9 ± 1.5[c]	32.3 ± 3.[4]b	0.496 ± 0.010[b]	2.62 ± 0.05[b]
AGH-4	181.4 ± 0.4[d]	124 ± 1[d]	0.351 ± 0.030[a]	1.94 ± 0.05[a]
Gallic acid	15.3 ± 7.8[e]	9.90 ± 5.82[a]	0.854 ± 0.020[c]	2.91 ± 0.07[b,c]
Trolox	66.3 ± 4.8[f]	41.9 ± 2.0[b]	0.515 ± 0.030[b]	2.58 ± 0.02[b]
Quercetin	19.2 ± 7.4[e]	4.63 ± 3.28[a]	0.496 ± 0.030[b]	2.99 ± 0.18[c]
Caffeic acid	26.6 ± 4.2[e]	21.1 ± 6.4[a,c]	0.768 ± 0.010[d]	2.77 ± 0.04[b,c]

[a]Normalized absorbance (A_{700} *per* concentration in μM). Values are presented as mean ± standard deviation (n = 3). Values followed by different superscript letters (a-f) in the same column correspond to significant differences by Tukey's test ($p < 0.05$). IC_{50}: concentration required to reduce 50% of the radical species; FRAP: Fe^{III} reduction assay; DPPH•: 2,2-diphenyl-2-picrylhydrazyl radical; ABTS•+: 2,2-azinobis(3-ethylbenzothiazoline-6-sulfonic acid.

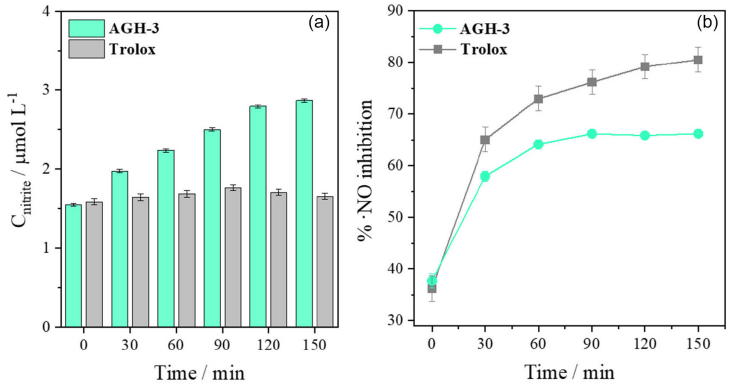

Figure 2. Graphs expressing the capacity of the aminoguanidine derivative **AGH-3** and the standard Trolox in sequestering the •NO radical. (a) Nitrite concentration formed as a function of reaction time. (b) Percentage of inhibition as a function of time.

heterocyclic, associated with the 3-hydrogen bonding centers, significantly increased the antioxidant activity of **AGH-3** with a relationship to the other compounds evaluated. Thus, a noteworthy observation is that having hydrogen bonds in compounds in the neutral form does not increase antioxidant activity; nevertheless, after hydrogen abstraction, radical stabilization becomes easier.[55] **AGH-2**, which also demonstrated efficacy against some of the evaluated radicals, has a strong electron-removal group (–CN), which might help stabilize the radical species formed.

In general, our studies indicated that the evaluated compounds present two mechanisms of antioxidant action: hydrogen atom transfer (HAT), i.e., activity via the $ABTS^{\bullet+}$ and $DPPH^{\bullet}$ method, and electron transfer, i.e., antioxidant activity via FRAP.[56] Thus, considering the excellent antioxidant activity in the methods evaluated, further antiproliferative activity against different human cancer cell strains was investigated.

Antiproliferative activity

According to the NCI-60 model to evaluate *in vitro* antiproliferative activity, the aminoguanidine derivatives were tested against a panel of tumor and non-tumor human cell lines (Table 2). The average activity against tumor cell lines evidenced that **AGH-3**, expressed as mean log(GI_{50}), was the most active aminoguanidine derivative, followed by **AGH-2** and **AGH-4** (mean log(GI_{50}) = 2). The **AGH-1** was inactive (GI_{50} > 900 μM for all cell lines). The most active compound was **AGH-3**, showing promising cytostatic effect against renal (786-0, GI_{50} = 6.3 μM), ovarian (OVCAR-03, GI_{50} = 11.0 μM), colorectal (HT-29, GI_{50} = 13.5 μM) adenocarcinomas and leukemia (K562, GI_{50} = 16.0 μM). Moreover, compounds **AGH-2**-**AGH-4** showed selectivity indexes (SI) lower than 3 for several cell lines.[57,58] Exceptions were **AGH-2** against 786-0 (SI = 8.9) and OVCAR-03 (SI = 2.8) cell lines (Table 2). The selectivity index refers to on-target toxicity,[59] suggesting that the aminoguanidine derivatives evaluated might induce *in vivo* some adverse effects related to cell growth inhibition in normal tissues, such as mucosa and bone marrow. Complementary *in vivo* evaluation is necessary to evaluate this hypothesis.

Data produced herein (Table 2) permit to rationalize the antiproliferative activity of **AGH-1-AGH-4** as associated, at least, with two factors: (*i*) the presence of hydrogen bond donor and acceptor centers and (*ii*) the electronic property associated with the presence of electron-withdrawing and electron acceptor groups. The compounds with antiproliferative activity maintained a 3/2 or 2/3 ratio between the centers of hydrogen bond donor and acceptor bonds. Moreover, electron-removal substituents in **AGH-1** and **AGH-2** derivatives reduced the cytostatic effect. In addition, similar results were described for caffeic acid ester derivatives.[60]

The annealing process led to an increase in the antiproliferative activity of **AGH-3** and **AGH-4**, being the indole derivative the most active. This result may have a relationship with the increased lipophilicity of the

Table 2. Antiproliferative profile of compounds **AGH-1-AGH-4** and doxorubicin (positive control)

Parameter	AGH-1		AGH-2		AGH-3		AGH-4		Doxorubicin	
	GI_{50} / μM	SI	GI_{50} / μM	SI	GI_{50} / μM	SI	GI_{50} / μM	SI	GI_{50} / μM	SI
U251	> 900	n.c.	164.0	1.5	20.4	0.6	96.3	0.9	0.48	1.0
MCF-7	> 900	n.c.	239.0	1.0	30.7	0.4	99.8	0.9	0.31	1.5
NCI-ADR/RES	> 900	n.c.	90.9	2.8	85.3	0.1	94.3	1.0	0.57	0.8
786-0	> 900	n.c.	28.0	8.9	6.3	2.0	91.2	1.0	0.09	5.3
NCI-H460	> 900	n.c.	289.0	0.9	15.1	0.8	99.0	0.9	0.18	2.7
PC-3	> 900	n.c.	314.0	0.8	28.1	0.5	98.4	0.9	1.43	0.3
OVCAR-03	> 900	n.c.	59.8	4.2	11.0	1.2	92.0	1.0	1.99	0.2
HT-29	> 900	n.c.	273.0	0.9	13.5	0.9	96.2	0.9	2.21	0.2
K562	> 900	n.c.	191.0	1.3	16.0	0.8	113.0	0.8	0.69	0.7
Mean log(GI_{50})	n.c.	n.c.	2.2	–	1.3	–	2.0	–	–0.2	–
HaCaT	> 900	–	250	–	12.7	–	90.1	–	0.48	–

GI_{50}: concentration required to elicit 50% of cell inhibition; SI: selectivity index: calculated as SI = ($GI_{50\,(HaCaT)}$)/($GI_{50\,tumor\,cell}$); [c]log GI_{50}: average antiproliferative activity expressed in logarithmic scale; n.c.: not calculated (GI_{50} values higher and/or lower than the experimental concentrations (0.25 to 250 μg mL^{-1} for **AGH-1**-**AGH-4**; 0.025 to 25 μg mL^{-1} for doxorubicin). Exposure time = 48 h. After the assays, GI_{50} values in μg mL^{-1} were normalized to μM. Human tumor cell lines: U251: glioblastoma; MCF-7: adenocarcinoma of the breast; NCI-ADR/RES: multidrug resistant ovarian adenocarcinoma; 786-0: adenocarcinoma of the kidney; NCI-H460: non-small cell carcinoma of the lung; PC-3: adenocarcinoma of the prostate; OVCAR-03: adenocarcinoma of the ovary; HT-29: colorectal adenocarcinoma; K562: chronic myelogenous leukemia; HaCaT: human non-tumor cell line immortalized keratinocyte.

compounds, allowing a greater penetration into the lipid bilayer of the cells.

Doxorubicin, the positive experimental control, is a nonselective anthracycline. The compound is described as a multitarget drug binding to topoisomerase enzyme II, intercalating DNA and inhibiting RNA polymerase I, thus, inducing cell death.[61] Based on the long-time evaluation of potential anticancer drugs, the NCI-60 model proposed that the antiproliferative profile might reflect the mechanism of action of a compound.[41] The differences observed among **AGH-1**-**AGH-4** and doxorubicin suggested that the new aminoguanidine derivatives may show various action mechanisms from doxorubicin. Different compounds with indole substituents have been reported as affecting cell proliferation by binding to DNA.[62,63] Thus, the interaction of the aminoguanidine derivative with an indole substituent (**AGH-3**) with a nucleic acid model was evaluated.

Interaction of **AGH-3** with ctDNA

UV-Vis studies

UV-Vis analysis of ctDNA in the absence and presence of potential ligands allows determining the formation of supramolecular complexes and possible structural changes in the macromolecule through spectral changes.[64,65] Thus, using this strategy, the uptake of free **AGH-3** at 310 nm (A_{AGH-3} = 0.5193), of ctDNA (A_{ctDNA} = 0.0491), and the **AGH-3**-ctDNA complex ($A_{complex}$ = 0.5566) were recorded (Figure 3a). These results suggested a complex formation between **AGH-3** and DNA, as the sum of the absorbance values of the ligand, and free ctDNA ($A_{AGH-3} + A_{ctDNA}$) was different than the absorbance values of the **AGH-3**-ctDNA complex ($A_{complex}$).[41,66]

Moreover, the development of the DNA-small molecules complex changes the magnitude of the absorbance band at 260 nm. This effect can be correlated with the strength of the interaction process and reflects structural variations in the ctDNA double helix when binding with ligand.[67,68] The observed hyperchromic effect during the spectrophotometric titration of **AGH-3** (Figure 3b) corroborates the occurrence of non-covalent interactions between the aminoguanidine derivative and the nucleic acid.[69]

Evaluation of **AGH-3**-ctDNA interaction by molecular fluorescence

The binding parameters for the **AGH-3** with ctDNA interaction were determined by fluorimetric titration. By adding increasing amounts of ctDNA to the **AGH-3** solution, a concentration-dependent in the fluorescent intensity was observed (Figure 4a). The data permitted us to rationalize that, due to the **AGH-3**-ctDNA interaction process, the rotation of the **AGH-3** was restricted and became more planar, increasing the overlap of the π orbitals and, thus, intensifying the fluorescent emission.[70,71]

Under physiological pH conditions, compound **AGH-3** (pK_{a1} = 1.93 (iminic group), pK_{a2} = 7.56 (imidazoline group), and pK_{a3} = 14.16 (indole group)) is distributed in the form of neutral (41%) and protonated (59%) species. The latter could bind to the DNA through electrostatic interactions and hydrogen bonding, contributing to the observed spectroscopic properties of the supramolecular complex. The binding constant (K_b) for the **AGH-3**-ctDNA complex was calculated from the linearization of a modified Benesi-Hildebrand equation:

$$\frac{1}{\Delta F} = \frac{1}{K_b \times \Delta F \times [ctDNA]} + \frac{1}{\Delta F} \quad (1)$$

where F and F_0 are the respective fluorescent intensities in the presence and absence of the species, thus $\Delta F = F - F_0$. K_b refers to the binding constant, and [ctDNA] to the

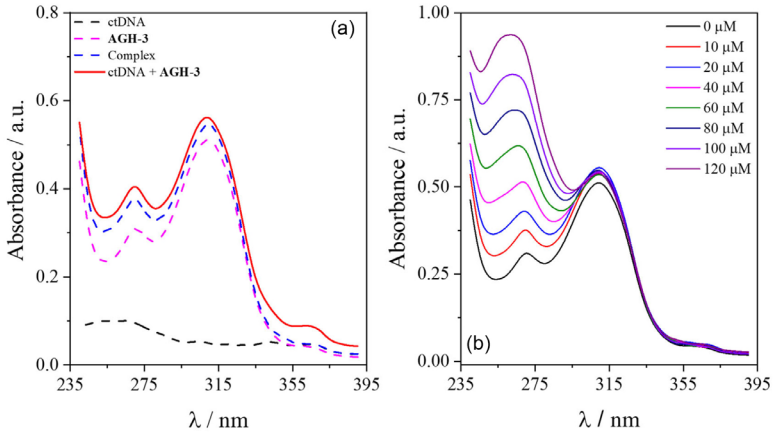

Figure 3. UV-Vis absorption spectra of the different systems. (a) ctDNA and **AGH-3** at 10 μM. (b) Spectrophotometric titration of **AGH-3** (10 μM) with different concentrations of ctDNA. Condition: pH = 7.4 in Tris-HCl 50 mM with NaCl 100 mM at 30 °C.

concentration of the macromolecule. The binding constant K_b was calculated as 2.89 (± 0.11) × 10^3 M^{-1} from linearization 1/ΔF *vs.* 1/[ctDNA] (Figure 4b). Compounds with an indole nucleus and different structural patterns presented K_b magnitudes from 3.80 × 10^3 to 4.17 × 10^7 M^{-1} when interacting with nucleic acid (ctDNA) under physiological conditions (Table S1, Supplementary Information section).

Fluorescence competition studies

Using classical probes Hoechst (HO, minor groove) and ethidium bromide (EB, intercalation), the mode of interaction between **AGH-3** and ctDNA was determined using a competition assay.[72-74] In the free form, both EB and HO present low fluorescence intensity in aqueous media. The interaction of both probes with the DNA double helix base pair results in increased fluorescence emission intensity.[75] Thus, reducing the fluorescence intensity of the DNA-probe complex induced by rising amounts of **AGH-3** in the solution would suggest that the evaluated compound has the same binding mode as the displaced probe (HO or EB). The magnitude of the fluorescence intensity suppression in the presence of **AGH-3** was calculated from the Stern-Volmer constant (K_{SV}):

$$\frac{F}{F_0} = 1 + K_{SV} \times [\textbf{AGH-3}] \quad (2)$$

where F_0 and F are, respectively, the fluorescence intensities in the absence and presence of **AGH-3**. The Stern-Volmer constant (K_{SV}) was determined from the slope obtained by linearization of the relationship (F_0/F) *vs.* [**AGH-3**]. Independent of the probe (HO or EB) used, the addition of **AGH-3** led to the suppression of fluorescent intensity in both probe-ctDNA systems (Figures 5a-5b). This indirectly affected the magnitude of the interaction process (K_b). The stoichiometries of the **AGH-3**-ctDNA (n) complex were calculated from the linearization of equation 3,[76,77] based on the log[(F_0 – F)/F] *vs.* log[**AGH-3**] (Figures 5c-5d).

$$\log\left(\frac{F_0 - F}{F}\right) = \log(K_b) + n\log[\textbf{AGH-3}] \quad (3)$$

The K_{SV} values for the EB-ctDNA (3.97(± 0.22) × 10^3 M^{-1}) and HO-ctDNA (2.23 (± 0.20) × 10^3 M^{-1}) systems, from titration with **AGH-3**, indicated that the ligand was able to displace both probes similarly, however with a particular preference for the intercalation binding mode (Table S2, Supplementary Information section). This behavior was also verified for the indirect binding constant, obtaining values of K_b = 2.59 (± 0.65) × 10^4 M^{-1} (EB-ctDNA) and 1.22 (± 0.72) × 10^4 M^{-1} (HO-ctDNA) (Table S2), indicating moderate ligand affinity for nucleic acid.[66] Santos-Junior *et al.*[78] evaluated thiazol-quinoline derivatives with the same probe-ctDNA systems used in this work and obtained K_{SV} values equal to 5.90 × 10^3 M^{-1} (EB-ctDNA) and 3.13 × 10^4 M^{-1} (HO-ctDNA) and K_b of 2.30 × 10^2 M^{-1} (EB-ctDNA) and 4.30 × 10^5 M^{-1} (HO-ctDNA), indicating greater ligand affinity for the minor groove region. Whereas Alves *et al.*[79] obtained K_{SV} values in the order of 10^4 M^{-1} for indole derivatives when using both intercalated competition (EB-ctDNA) and minor groove (4',6-diamidino-2-phenylindole-(DAPI)-ctDNA) systems. Thus, to determine the relative affinity and confirm the preferred mode of interaction, the intercalative probability of **AGH-3** was calculated,[80] which revealed a 62% preference for the intercalation binding mode (Table S2), corroborating the values of Ksv and Kb previously presented. Finally, the values of n for the two systems evaluated were approximately 1,

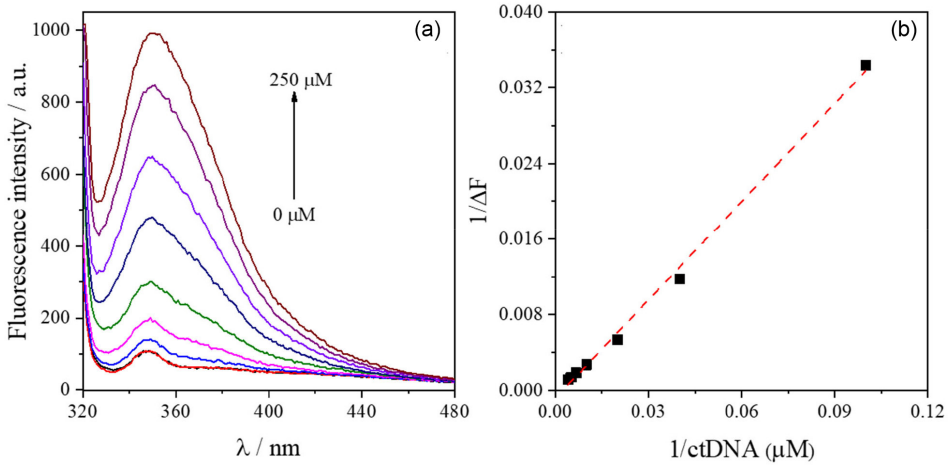

Figure 4. Evaluation of **AGH-3**-ctDNA interaction by molecular fluorescence (condition: pH = 7.4, Tris-HCl 50 mM, NaCl 100 mM) at 30 °C. (a) Spectra of **AGH-3** (10 µM) with increasing additions (1, 10, 25, 50, 100, 150, 200, and 250 µM) of ctDNA. (b) Graph of 1/ΔF *vs.* 1/[ctDNA] used for K_b determination.

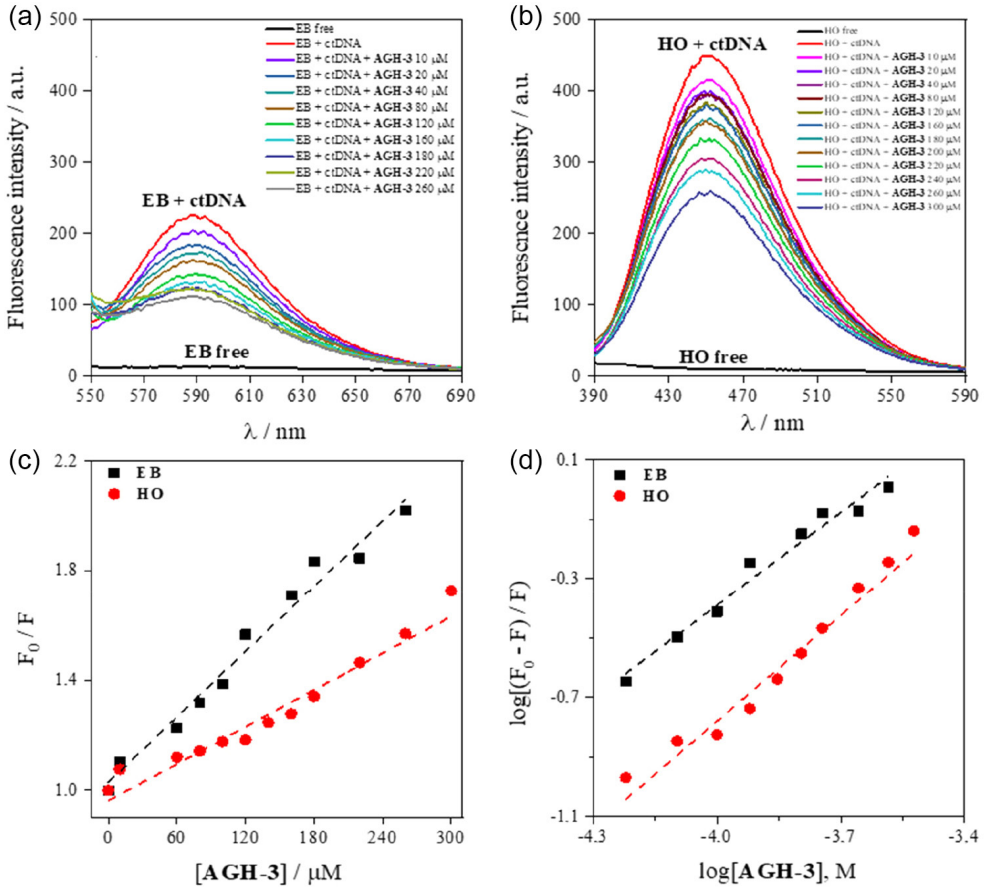

Figure 5. Evaluation of the **AGH-3**-ctDNA interaction mode (condition: pH = 7.4, Tris-HCl 50 mM, NaCl 100 mM) at 30 °C. (a) Equilibrium competition of **AGH-3** with the EB-ctDNA complex. (b) Equilibrium competition of **AGH-3** with the HO-ctDNA complex. (c) Stern-Volmer plot for **AGH-3**. (d) The logarithmic curve for the calculation of the binding constant of **AGH-3** with ctDNA.

demonstrating that the **AGH-3**-ctDNA interaction occurs with a stoichiometric ratio of 1:1 (Table S2).

DNA thermal denaturation studies

The DNA double helix can be stabilized by hydrogen bonds and stacking interactions between the purine and pyrimidine bases that make up the macromolecule. An increase in temperature leads to the weakening of these forces that stabilize the helical structure of the macromolecule, thus producing the base pairs separation and the single-strand DNA formation. This process is known as thermal DNA denaturation, and the temperature value (T_m) where 50% of the DNA is in single-stranded form and 50% of the DNA is in double-stranded form is used as a parameter to evaluate the binding mode.[76,81] Thus, when small molecules interact with DNA, variations in the T_m value may occur, depending on the preferential binding mode. The T_m value for free ctDNA and the **AGH-3**-ctDNA complex were 76.2 and 82.2 °C (ΔT_m = 6 °C), respectively (Figure S14, Supplementary Information section). Thus, since ΔT_m > 5 ºC, there is an indication that the preferential binding mode of **AGH-3**-ctDNA would be by intercalation,[82] corroborating the spectroscopy studies based on competition assays.

Docking molecular studies

Molecular docking results are often used to predict or prove the interaction between a ligand and a target molecule, as in the case of the ligand **AGH-3** and DNA.[83,84] Although the accuracy of docking predictions depends on the quality of the molecular structure models used, the energy parameters, and the calculation methods used, these predictions are often able to provide useful information about the molecular interaction.

In this specific case, the molecular docking results suggest that the **AGH-3** ligand interacts with base pairs in the major groove of the DNA, and also between these base pairs, through a combination of van der Waals bonds, hydrogen bonds, and π-anion interactions (Figure S15, Supplementary Information section). Furthermore, the interaction **ΔG** value of −7.7 KJ mol^{-1} suggests that the affinity energy between the **AGH-3**-DNA complex is favorable. Thus, since the experimental results also showed that the **AGH-3** ligand interacts with DNA at the positions

predicted by the molecular docking model, it can be stated that the theoretical results corroborated with experimental results.

Conclusions

The synthesis and characterization of new aminoguanidine derivatives were described with one compound, **AGH-3**, presenting promisor biological activities. It also showed antioxidant and antiproliferative activities together with DNA binding affinity, and these effects were attributed to indole substituent in the aminoguanidine hydrazone skeleton. Finally, further pre-clinical assays may confirm the *in vitro* evidence.

Supplementary Information

Supplementary data are available free of charge at http://jbcs.sbq.org.br as PDF file.

Acknowledgments

The authors thank the Universidade Federal de Alagoas (UFAL), Frederick Cancer Research & Development Center, National Cancer Institute, Frederick, MA, USA and Dr Ricardo Della Coletta (University of Campinas) for donating the cell K562 (chronic myelogenous leukemia) and HaCat (human keratinocyte), respectively. They also acknowledge the following institutions: Coordenação de Aperfeiçoamento de Pessoal de Nível Superior - Brazil (CAPES) - Finance Code 001, Financiadora de Estudos e Projetos (FINEP), and Conselho Nacional de Desenvolvimento Científico e Tecnológico (CNPq) (process number 465516/2014-0), for financial support; and research fellowships: MAF, JXAJ, ALTGR, and JCCS, Fundação de Amparo à Pesquisa do Estado de Alagoas (FAPEAL). The authors ALTGR and MAF also grant CNPq for Productivity Scholarship in Technological Development and Innovative Extension.

Author Contributions

Ari S. Guimarães was responsible for conceptualization, investigation, methodology, writing original draft; Woodland S. Oliveira for investigation, methodology, writing original draft; Aline R. S. Araújo for investigation, methodology; Mary Ann Foglio for investigation, methodology, writing review and editing; Ana Lucia Ruiz for investigation, methodology, writing original draft; Pedro Gregório V. Aquino for formal analysis, investigation, methodology, validation, writing-original draft, review and editing; Martine Schmitt for formal analysis, investigation, methodology, project administration, supervision, writing-original draft, review and editing; Joao Araujo Jr. for formal analysis, funding acquisition, investigation, methodology, project administration, validation, writing-original draft, review and editing; Isis Figueiredo for investigation, methodology, project administration, visualization, writing original draft; Josue Santos for conceptualization, formal analysis, project administration, supervision, visualization, writing-original draft, review and editing.

References

1. da Silva, M. P. G.; de Oliveira, Y. M.; Candido, A. C. L.; de Araújo-Júnior, J. X.; Rodrigues, É. E. S.; Monteiro, K. L. C.; de Aquino, T. M.; de Abreu, F. C.; *J. Biomater. Nanobiotechnol.* **2020**, *11*, 33. [Crossref]
2. Song, M.; Wang, S.; Wang, Z.; Fu, Z.; Zhou, S.; Cheng, H.; Liang, Z.; Deng, X.; *Eur. J. Med. Chem.* **2019**, *166*, 108. [Crossref]
3. Andrade, G. R.; Kunsminskas, J.; Pizzuti, L.; dos Anjos, A.; Inglez, S. D.; Tirloni, B.; Suegama, P. H.; *Inorg. Chem. Commun.* **2015**, *61*, 210. [Crossref]
4. Sidoryk, K.; Switalska, M.; Jaromin, A.; Cmoch, P.; Bujak, I.; Kaczmarska, M.; Wietrzyk, J.; Dominguez, E. G.; Zarnowski, R.; Andes, D. R.; Bankowski, K.; Cybulski, M.; Kaczmarek, L.; *Eur. J. Med. Chem.* **2015**, *105*, 208. [Crossref]
5. Paesano, N.; Marzocco, S.; Vicidomini, C.; Saturnino, C.; Autore, G.; De Martino, G.; Sbardella, G.; *Bioorg. Med. Chem. Lett.* **2005**, *15*, 539. [Crossref]
6. Zamperini, C.; MacCari, G.; Deodato, D.; Pasero, C.; D'Agostino, I.; Orofino, F.; De Luca, F.; Dreassi, E.; Docquier, J. D.; Botta, M.; *Sci. Rep.* **2017**, *7*, 8251. [Crossref]
7. Pasero, C.; D'Agostino, I.; De Luca, F.; Zamperini, C.; Deodato, D.; Truglio, G. I.; Sannio, F.; Del Prete, R.; Ferraro, T.; Visaggio, D.; Mancini, A.; Guglielmi, M. B.; Visca, P.; Docquier, J. D.; Botta, M.; *J. Med. Chem.* **2018**, *61*, 9162. [Crossref]
8. Kim, S. H.; Semenya, D.; Castagnolo, D.; *Eur. J. Med. Chem.* **2021**, *216*, 113293. [Crossref]
9. Baum, T.; Shropshire, A. T.; Rowles, G.; Van Pelt, T. R.; Fernandez, S. P.; Eckfeld, D. K.; Gluckman, M. I.; *J. Pharmacol. Exp. Ther.* **1970**, *171*, 276. [Link] accessed in October 2023
10. Li, T.; Yang, S.; She, X.; Yan, Q.; Zhang, P.; Zhu, H.; Wang, F.; Luo, X.; Sun, X.; *Br. J. Pharmacol.* **2019**, *176*, 801. [Crossref]
11. Martynowicz, J.; Doggett, J. S.; Sullivan Jr., W. J.; *Antimicrob. Agents Chemother.* **2020**, *64*. [Crossref]
12. Martynowicz, J.; Augusto, L.; Wek, R. C.; Boehm, S. L.; Sullivan, W. J.; *mBio* **2019**, *10*. [Crossref]
13. Callejo, G.; Pattison, L. A.; Greenhalgh, J. C.; Chakrabarti, S.; Andreopoulou, E.; Hockley, J. R. F.; Smith, E. S. J.; Rahman, T.; *Biochem. Pharmacol.* **2020**, *174*, 113834. [Crossref]
14. Xie, W.; Xie, J.; Vince, R.; More, S. S.; *Chem. Res. Toxicol.* **2020**, *33*, 162. [Crossref]

15. Ho, K.-H.; Lee, Y.-T.; Chen, P.-H.; Shih, C.-M.; Cheng, C.-H.; Chen, K.-C.; *Neurotherapeutics* **2021**, *18*, 1371. [Crossref]
16. Ruiz, A.; Zuazo, J.; Ortiz-Sanz, C.; Luchena, C.; Matute, C.; Alberdi, E.; *Int. J. Mol. Sci.* **2020**, *21*, 6088. [Crossref]
17. Fusade-Boyer, M.; Dupré, G.; Bessière, P.; Khiar, S.; Quentin-Froignant, C.; Beck, C.; Lecollinet, S.; Rameix-Welti, M.-A.; Eléouët, J.-F.; Tangy, F.; Lajoie, B.; Bertagnoli, S.; Vidalain, P.-O.; Gallardo, F.; Volmer, R.; *Front. Immunol.* **2019**, *10*, 134. [Crossref]
18. LaFrate, A. L.; Gunther, J. R.; Carlson, K. E.; Katzenellenbogen, J. A.; *Bioorg. Med. Chem.* **2008**, *16*, 10075. [Crossref]
19. Messeder, J. C.; Tinoco, L. W.; Figueroa-Villar, J. D.; Souza, E. M.; Santa Rita, R.; de Castro, S. L.; *Bioorg. Med. Chem. Lett.* **1995**, *5*, 3079. [Crossref]
20. Santana, C. C.; Silva-Júnior, E. F.; Santos, J. C. N.; Rodrigues, É. E. S.; da Silva, I. M.; Araújo-Júnior, J. X.; do Nascimento, T. G.; Oliveira Barbosa, L. A.; Dornelas, C. B.; Figueiredo, I. M.; Santos, J. C. C.; Grillo, L. A. M.; *Bioorg. Chem.* **2019**, *87*, 169. [Crossref]
21. França, P. H. B.; da Silva-Júnior, E. F.; Aquino, P. G. V.; Santana, A. E. G.; Ferro, J. N. S.; de Oliveira Barreto, E.; do Ó Pessoa, C.; Meira, A. S.; de Aquino, T. M.; Alexandre-Moreira, M. S.; Schmitt, M.; de Araújo-Júnior, J. X.; *Acta Pharm.* **2016**, *66*, 129. [Crossref]
22. Sandes, S. M. S.; Heimfarth, L.; Brito, R. G.; Santos, P. L.; Gouveia, D. N.; Carvalho, A. M. S.; Quintans, J. S. S.; da Silva-Júnior, E. F.; de Aquino, T. M.; França, P. H. B.; de Araújo-Júnior, J. X.; Albuquerque-Júnior, R. L. C.; Zengin, G.; Schmitt, M.; Bourguignon, J.-J.; Quintans-Júnior, L. J.; *Chem.-Biol. Interact.* **2018**, *286*, 1. [Crossref]
23. Heimfarth, L.; Carvalho, A. M. S.; Quintans, J. S. S.; Pereira, E. W. M.; Lima, N. T.; Carvalho, M. T. B.; Barreto, R. S. S.; Moreira, J. C. F.; da Silva-Júnior, E. F.; Schmitt, M.; Bourguignon, J.-J.; de Aquino, T. M.; de Araújo-Júnior, J. X.; Quintans-Júnior, L. J.; *Neurochem. Int.* **2020**, *134*, 104647. [Crossref]
24. Sztanke, K.; Rzymowska, J.; Niemczyk, M.; Dybała, I.; Kozioł, A. E.; *Eur. J. Med. Chem.* **2006**, *41*, 1373. [Crossref]
25. Sztanke, K.; Fidecka, S.; Kędzierska, E.; Karczmarzyk, Z.; Pihlaja, K.; Matosiuk, D.; *Eur. J. Med. Chem.* **2005**, *40*, 127. [Crossref]
26. Pereira, C. N.; Rosa, J. O.; Lara, L. S.; Orlando, L. M. R.; Figueiredo, N. S.; Pereira, M. C. S.; Nobuyasu Jr., R. S. N.; dos Santos, M. S.; *J. Mol. Struct.* **2023**, *1290*, 135899. [Crossref]
27. Caputto, M. E.; Ciccarelli, A.; Frank, F.; Moglioni, A. G.; Moltrasio, G. Y.; Vega, D.; Lombardo, E.; Finkielsztein, L. M.; *Eur. J. Med. Chem.* **2012**, *55*, 155. [Crossref]
28. Hammoud, H.; Elhabazi, K.; Quillet, R.; Bertin, I.; Utard, V.; Laboureyras, E.; Bourguignon, J. J.; Bihel, F.; Simonnet, G.; Simonin, F.; Schmitt, M.; *ACS Chem. Neurosci.* **2018**, *9*, 2599. [Crossref]
29. Granja, B. S.; de Mendonça Filho, J. R.; Oliveira, W. S.; Santos, J. C. C.; *Anal. Methods* **2018**, *10*, 2197. [Crossref]
30. Oliveiraa, W. S.; Santos, J. C. C.; *J. Braz. Chem. Soc.* **2020**, *31*, 2479. [Crossref]
31. Das, S.; da Silva, C. J.; Silva, M. M.; Dantas, M. D. A.; de Fátima, Â.; Góis Ruiz, A. L. T.; da Silva, C. M.; de Carvalho, J. E.; Santos, J. C. C.; Figueiredo, I. M.; da Silva-Júnior, E. F.; de Aquino, T. M.; de Araújo-Júnior, J. X.; Brahmachari, G.; Modolo, L. V.; *J. Adv. Res.* **2018**, *9*, 51. [Crossref]
32. Krezel, I.; Mikiciuk-Olasik, E.; Zurek, E.; Glówka, M. L.; *Pharm. Pharmacol. Commun.* **1999**, *5*, 485. [Crossref]
33. Karaghiosoff, K.; Klapo, T. M.; Mayer, P.; Piotrowski, H.; Polborn, K.; Willer, R. L.; Weigand, J. J.; *J. Org. Chem.* **2006**, *71*, 1295. [Crossref]
34. Shao, Y.; Ding, Y.; Jia, Z.-L.; Lu, X.-M.; Ke, Z.-H.; Xu, W.-H.; Lu, G.-Y.; *Bioorg. Med. Chem.* **2009**, *17*, 4274. [Crossref]
35. Ulrich, P.; Cerami, A.; *J. Med. Chem.* **1984**, *27*, 35. [Crossref]
36. Foye, W. O.; Almassian, B.; Eisenberg, M. S.; Maher, T. J.; *J. Pharm. Sci.* **1990**, *79*, 527. [Crossref]
37. Gülçin, I.; Bursal, E.; Sehitoğlu, M. H.; Bilsel, M.; Gören, A. C.; *Food Chem. Toxicol.* **2010**, *48*, 2227. [Crossref]
38. Maia, R. M.; Moura, C. W. N.; Bispo, V. S.; Santos, J. L. A.; Santana, R. S.; Matos, H. R.; *Rev. Bras. Farmacogn.* **2010**, *20*, 489. [Crossref]
39. *OriginPro*, version 9.0; OriginLab Corporation, Northampton, Massachusetts, USA, 2009.
40. Monks, A.; Scudiero, D.; Skehan, P.; Shoemaker, R.; Paull, K.; Vistica, D.; Hose, C.; Langley, J.; Cronise, P.; Vaigro-Wolff, A.; Gray-Goodrich, M.; Campbell, H.; Mayo, J.; Boyd, M.; *J. Natl. Cancer Inst.* **1991**, *83*, 757. [Crossref]
41. Shoemaker, R. H.; *Nat. Ver. Cancer* **2006**, *6*, 813. [Crossref]
42. Silva, M. M.; Savariz, F. C.; Silva, E. F.; de Aquino, T. M.; Sarragiotto, M. H.; Santos, J. C. C.; Figueiredo, I. M.; *J. Braz. Chem. Soc.* **2016**, *27*, 1558. [Crossref]
43. *ChemDraw*, version 15.1.; PerkinElmer Informatics, Inc., Massachusetts, USA, 2016.
44. Stewart, J. J. P.; *MOPAC*, version 2016; Stewart Computational Chemistry, Colorado, USA, 2007.
45. Macrae, C. F.; Bruno, I. J.; Chisholm, J. A.; Edgington, P. R.; McCabe, P.; Pidcock, E.; Rodriguez-Monge, L.; Taylor, R.; Van De Streek, J.; Wood, P. A.; *Mercury*, version 2022.1.0.; Cambridge Crystallographic Data Centre, Inc., Massachusetts, USA, 2007.
46. Trott, O.; Olson, A. J.; *Autodock Tools*, version 1.5.6.; California, USA, 2009.
47. Silva, M. M.; Nascimento, E. O. O.; Silva Jr., E. F.; de Araújo Jr., J. X.; Santana, C. C.; Grillo, L. A. M.; de Oliveira, R. S.; Costa, P. R. R.; Buarque, C. D.; Santos, J. C. C.; Figueiredo, I. M.; *Int. J. Biol. Macromol.* **2017**, *96*, 223. [Crossref]
48. *Discovery Studio Visualizer*, version 21.1.0.20298; BIOVIA, Dassault Systèmes, San Diego, California, USA, 2021.
49. Pettersen, E. F.; Goddard, T. D.; Huang, C. C.; Couch, G. S.; Greenblatt, D. M.; Meng, E. C.; Ferrin, T. E.; *UCSF Chimera*,

version 1.15; Resource for Biocomputing, Visualization, and Informatics at the University of California, San Francisco, California, USA, 2004.
50. Sztanke, M.; Kandefer-Szerszeń, M.; Sztanke, K.; *Free Radical Res.* **2018**, *52*, 685. [Crossref]
51. Baldisserotto, A.; Demurtas, M.; Lampronti, I.; Tacchini, M.; Moi, D.; Balboni, G.; Pacifico, S.; Vertuani, S.; Manfredini, S.; Onnis, V.; *Bioorg. Chem.* **2020**, *94*, 103396. [Crossref]
52. Faillace, M. S.; Silva, A. P.; Alves Borges Leal, A. L.; da Costa, L.; Barreto, H. M.; Peláez, W. J.; *Chem. Med. Chem.* **2020**, *15*, 851. [Crossref]
53. Mihailović, N.; Marković, V.; Matić, I. Z.; Stanisavljević, N. S.; Jovanović, Ž. S.; Trifunović, S.; Joksović, L.; *RSC Adv.* **2017**, *7*, 8550. [Crossref]
54. Solaiman, M. A.; Ali, M. A.; Abdel-Moein, N. M.; Mahmoud, E. A.; *Biocatal. Agric. Biotechnol.* **2020**, *29*, 101832. [Crossref]
55. Scotti, L.; Scotti, M. T.; Cardoso, C.; Pauletti, P.; Castro-Gamboa, I.; Bolzani, V. D. S.; Velasco, M. V. R.; Menezes, C. M. D. S.; Ferreira, E. I.; *Rev. Bras. Cienc. Farm.* **2007**, *43*, 153. [Crossref]
56. Gulcin, İ.; *Arch. Toxicol*. **2020**, *94*, 651. [Crossref]
57. Hassan, G. S.; Georgey, H. H.; Mohammed, E. Z.; George, R. F.; Mahmoud, W. R.; Omar, F. A.; *Eur. J. Med. Chem.* **2021**, *218*, 113389. [Crossref]
58. El-Miligy, M. M. M.; Rida, S. M.; Ashour, F. A.; Badr, M. H.; El-Bassiony, E. M.; El-Demellawy, M. A.; Omar, A. M.; *Future Sci.* **2018**, *4*. [Crossref]
59. Muller, P. Y.; Milton, M. N.; *Nat. Rev. Drug Discovery* **2012**, *11*, 751. [Crossref]
60. Xie, J.; Yang, F.; Zhang, M.; Lam, C.; Qiao, Y.; Xiao, J.; Zhang, D.; Ge, Y.; Fu, L.; Xie, D.; *Bioorg. Med. Chem. Lett.* **2017**, *27*, 131. [Crossref]
61. Tacar, O.; Sriamornsak, P.; Dass, C. R.; *J. Pharm. Pharmacol.* **2013**, *65*, 157. [Crossref]
62. Lončar, B.; Perin, N.; Mioč, M.; Boček, I.; Grgić, L.; Kralj, M.; Tomić, S.; Stojković, M. R.; Hranjec, M.; *Eur. J. Med. Chem.* **2021**, *217*, 113342. [Crossref]
63. Lafayette, E. A.; de Almeida, S. M. V.; Santos, R. V. C.; de Oliveira, J. F.; Amorim, C. A. C.; da Silva, R. M. F.; Pitta, M. G. R.; Pitta, I. R.; de Moura, R. O.; de Carvalho Jr., L. B.; Rêgo, M. J. B. M.; de Lima, M. C. A.; *Eur. J. Med. Chem.* **2017**, *136*, 511. [Crossref]
64. Sirajuddin, M.; Ali, S.; Badshah, A.; *J. Photochem. Photobiol., B* **2013**, *124*, 1. [Crossref]
65. Wang, R.; Hu, X.; Pan, J.; Zhang, G.; Gong, D.; *J. Mol. Liq.* **2019**, *282*, 356. [Crossref]
66. Wu, J.; Cui, G.; Zhao, M.; Cui, C.; Peng, S.; *Mol. BioSyst.* **2007**, *3*, 855. [Crossref]
67. Afrin, S.; Rahman, Y.; Sarwar, T.; Husain, M. A.; Ali, A.; Shamsuzzaman; Tabish, M.; *Spectrochim. Acta, Part A* **2017**, *186*, 66. [Crossref]
68. Thomas, R. K.; Sukumaran, S.; Sudarsanakumar, C.; *J. Mol. Struct.* **2019**, *1178*, 62. [Crossref]
69. Rehman, S. U.; Sarwar, T.; Husain, M. A.; Ishqi, H. M.; Tabish, M.; *Arch. Biochem. Biophys.* **2015**, *576*, 49. [Crossref]
70. da Silva, C. M.; Silva, M. M.; Reis, F. S.; Ruiz, A. L. T. G.; de Carvalho, J. E.; Santos, J. C. C.; Figueiredo, I. M.; Alves, R. B.; Modolo, L. V; de Fátima, Â.; *J. Photochem. Photobiol., B* **2017**, *172*, 129. [Crossref]
71. Han, L.; Zhou, Y.; Huang, X.; Xiao, M.; Zhou, L.; Zhou, J.; Wang, A.; Shen, J.; *Spectrochim. Acta, Part A* **2014**, *123*, 497. [Crossref]
72. Husain, M. A.; Ishqi, H. M.; Sarwar, T.; Rehman, S. U.; Tabish, M.; *MedChemComm* **2017**, *8*, 1283. [Crossref]
73. Huang, S.; Zhu, F.; Xiao, Q.; Liang, Y.; Zhou, Q.; Su, W.; *RSC Adv.* **2015**, *5*, 42889. [Crossref]
74. Prieto, D.; Aparicio, G.; Morande, P. E.; Zolessi, F. R.; *Histochem. Cell Biol.* **2014**, *142*, 335. [Crossref]
75. Mirzaei-Kalar, Z.; *J. Pharm. Biomed. Anal.* **2018**, *161*, 101. [Crossref]
76. Qais, F. A.; Ahmad, I.; *J. Pharm. Biomed. Anal.* **2018**, *149*, 193. [Crossref]
77. Kalaivani, P.; Prabhakaran, R.; Kaveri, M. V.; Huang, R.; Staples, R. J.; Natarajan, K.; *Inorg. Chim. Acta* **2013**, *405*, 415. [Crossref]
78. Santos-Junior, P. F. S.; Nascimento, I. J. S.; da Silva, E. C. D.; Monteiro, K. L. C.; de Freitas, J. D.; de Lima Lins, S.; Maciel, T. M. S.; Cavalcanti, B. C.; José de, J. B.; de Abreu, F. C.; Figueiredo, I. M.; Carinhanha C. Santos, J.; Pessoa, C. Ó.; da Silva-Júnior, E. F.; de Araújo-Júnior, J. X.; de Aquino, T. M.; *N. J. Chem.* **2021**, *45*, 13847. [Crossref]
79. Alves, J. E. F.; de Oliveira, J. F.; de Lima Souza, T. R. C.; de Moura, R. O.; de Carvalho Jr., L. B.; Alves de Lima, M. C.; de Almeida, S. M. V.; *Int. J. Biol. Macromol.* **2021**, *170*, 622. [Crossref]
80. Phadte, A. A.; Banerjee, S.; Mate, N. A.; Banerjee, A.; *Biochem. Biophys. Rep.* **2019**, *18*, 100629. [Crossref]
81. Qais, F. A.; Abdullah, K. M.; Alam, Md. M.; Naseem, I.; Ahmad, I.; *Int. J. Biol. Macromol.* **2017**, *97*, 392. [Crossref]
82. Hussain, I.; Fatima, S.; Siddiqui, S.; Ahmed, S.; Tabish, M.; *Spectrochim. Acta, Part A* **2021**, *260*, 119952. [Crossref]
83. Stanzione, F.; Giangreco, I.; Cole, J. C. In *Progress in Medicinal Chemistry*, vol. 60, 1st ed.; Witty, D. R.; Cox, B., eds.; Elsevier: London, UK, 2021. [Crossref]
84. Meng, X.-Y.; Zhang, H.-X.; Mezei, M.; Cui, M.; *Curr. Comput.-Aided Drug Des.* **2011**, *7*, 146. [Crossref]

Submitted: June 17, 2023
Published online: November 7, 2023